Weak ergodicity breaking in the Schwinger model

Jean-Yves Desaules [1] Debasish Banerjee [2,3] Ana Hudomal [1,4] Zlatko Papić [1] Arnab Sen [5] and Jad C. Halimeh [6,7,*]

[1]*School of Physics and Astronomy, University of Leeds, Leeds LS2 9JT, United Kingdom*
[2]*Theory Division, Saha Institute of Nuclear Physics, 1/AF Bidhan Nagar, Kolkata 700064, India*
[3]*Homi Bhabha National Institute, Training School Complex, Anushaktinagar, Mumbai 400094, India*
[4]*Institute of Physics Belgrade, University of Belgrade, 11080 Belgrade, Serbia*
[5]*School of Physical Sciences, Indian Association for the Cultivation of Science, Kolkata 700032, India*
[6]*Department of Physics and Arnold Sommerfeld Center for Theoretical Physics (ASC), Ludwig-Maximilians-Universität München,*
Theresienstraße 37, D-80333 München, Germany
[7]*Munich Center for Quantum Science and Technology (MCQST), Schellingstraße 4, D-80799 München, Germany*

As a paradigm of weak ergodicity breaking in disorder-free nonintegrable models, quantum many-body scars (QMBS) can offer deep insights into the thermalization dynamics of gauge theories. Having been first discovered in a spin-$\frac{1}{2}$ quantum link formulation of the Schwinger model, it is a fundamental question as to whether QMBS persist for $S > \frac{1}{2}$ since such theories converge to the lattice Schwinger model in the large-S limit, which is the appropriate version of lattice QED in one spatial dimension. In this work, we address this question by exploring QMBS in spin-S U(1) quantum link models (QLMs) with staggered fermions. We find that QMBS persist at $S > \frac{1}{2}$, with the resonant scarring regime, which occurs for a zero-mass quench, arising from simple high-energy gauge-invariant initial product states. We furthermore find evidence of detuned scarring regimes, which occur for finite-mass quenches starting in the physical vacua and the charge-proliferated state. Our results conclusively show that QMBS exist in a wide class of lattice gauge theories in one spatial dimension represented by spin-S QLMs coupled to dynamical fermions, and our findings can be tested on near-term cold-atom quantum simulators of these models.

Introduction. Quantum many-body scars (QMBS) form an intriguing paradigm of ergodicity breaking in interacting systems that are typically expected to thermalize due to their nonintegrability and spatial homogeneity [1–8]. QMBS comprise eigenstates of low entanglement entropy [9,10], many of which reside in the middle of the spectrum, and are often separated roughly equally in energy [11,12]. These eigenstates are nonthermal, forming a "cold" subspace that is weakly connected to the rest of the Hilbert space. Consequently, quenches starting in initial states with high overlap with these nonthermal states do not show typical thermalization, but instead exhibit long-lived coherent dynamics [13,14]. This behavior is of particular interest to fundamental investigations of the eigenstate thermalization hypothesis (ETH) [15–20], as it has been linked to novel mechanisms for avoiding thermalization in closed quantum systems based on spectrum generating algebras [21–24] and embedding of nonthermal eigenstates [25] (see recent reviews [26,27]). Moreover, given that QMBS constitute high- or even infinite-temperature states, when the system is initially prepared in them it will not dephase its

information, which is pertinent to applications in quantum memory and information processing [28–31].

QMBS are also relevant to gauge theories [32–36], which describe the interactions of elementary particles mediated by gauge bosons through an extensive set of local constraints [37–39]. A paradigmatic example of the latter is Gauss's law in quantum electrodynamics (QED), where the distribution of charged matter strictly specifies the allowed configurations of the surrounding electromagnetic field [40]. Recently, a concerted experimental effort has emerged for the implementation of gauge theories in synthetic quantum matter (SQM) devices [41–51]. This has been facilitated in large part due to the great progress achieved in the precision and control of SQM setups [52,53], making the quantum simulation of gauge theories a realistic endeavor [54–60]. Due to the complexity of these experiments, the implementations often focus on quantum link formulations of gauge theories, where spin-S operators model the gauge fields, which in QED span an infinite-dimensional Hilbert space [61]. This has allowed the first large-scale realization of the spin-$\frac{1}{2}$ U(1) quantum link model (QLM) in $1 + 1$ dimensions [$(1 + 1)$D] using ultracold atoms [50,51].

The first experimental observation of QMBS was achieved in a Rydberg-atom setup implementing the PXP model [1], a paradigm of QMBS which maps to the spin-$\frac{1}{2}$ U(1) QLM [33]. Such a mapping breaks down at $S > \frac{1}{2}$, and it remains an open question whether QMBS persist at larger link spin lengths in the QLM formulation of QED, and, if they do, what their form will be. In this Letter, we show that QMBS are ubiquitous in

lattice gauge theories for all values of spin $S \leqslant \frac{5}{2}$ accessible in numerical simulations. For a zero-mass quench, QMBS arise when the system is prepared in the *extreme vacua* of the spin-S U(1) QLM, which are the most highly excited vacuum states of lattice QED. Furthermore, we find that preparing the system in the physical (least excited) vacua or in the charge-proliferated state can still lead to *detuned* scarring behavior for certain massive quenches, similar to the case of $S = \frac{1}{2}$ that has recently been demonstrated experimentally in a tilted Bose-Hubbard optical lattice [7]. The nonthermalizing dynamics due to QMBS provides a useful benchmark for the upcoming realizations of larger-S lattice gauge theories in cold-atom quantum simulators and the exploration of their out-of-equilibrium properties [48,57].

U(1) quantum link model. The Schwinger model, or QED in $1 + 1$ dimensions, is possibly the simplest gauge theory with dynamical matter that shows nontrivial phenomena like confinement [62,63]. A discrete version of the Schwinger Hamiltonian on a lattice is provided by the Kogut-Susskind formulation, which is also reached in the large-S limit of the QLMs being studied here. The $(1 + 1)$D spin-S U(1) QLM is given by the Hamiltonian [64,65]

$$\hat{H} = \sum_{j=1}^{L} \left[\frac{J}{2a\sqrt{S(S+1)}} (\hat{\sigma}_j^+ \hat{s}_{j,j+1}^+ \hat{\sigma}_{j+1}^- + \text{H.c.}) + \frac{\mu}{2}(-1)^j \hat{\sigma}_j^z + \frac{g^2 a}{2} (\hat{s}_{j,j+1}^z)^2 \right].$$

(1)

Here, $J = 1$ sets the energy scale, μ is the fermionic mass, and g^2 is the gauge coupling strength. Throughout this work, we will set the lattice spacing to $a = 1$ and employ periodic boundary conditions, with L denoting the number of lattice sites. The matter field on site j is represented by the Pauli operator $\hat{\sigma}_j^z$, and the electric (gauge) field at the link between sites j and $j + 1$ is represented by the spin-S operator $\hat{s}_{j,j+1}^{z(+)}$. The generator of the U(1) gauge symmetry of Hamiltonian (1) is

$$\hat{G}_j = \frac{\hat{\sigma}_j^z + (-1)^j}{2} + \hat{s}_{j-1,j}^z - \hat{s}_{j,j+1}^z,$$

(2)

which can be interpreted as a discretized version of Gauss's law relating the matter occupation on site j to the electric-field configuration on its neighboring links. We will work in the *physical* sector of Gauss's law: $\hat{G}_j |\phi\rangle = 0, \ \forall \ j$.

Due to the gauge symmetry imposed by the generator (2), one can integrate out the matter fields in the Hamiltonian (1), resulting in a constrained spin system. For $S = \frac{1}{2}$, this corresponds to the PXP model [33]. For larger S, the resulting model differs from generalizations of the PXP model already explored in the literature [13,66]. In the companion article [67], we derive the relevant constrained spin-S model corresponding to the spin-S U(1) QLM for any value of S [68]. Exact diagonalization (ED) techniques resolving the translation and spatial-inversion symmetries have been employed to study the eigenstates of these models. Time-evolution results are obtained either directly from the ED results or by time evolving the initial state using sparse matrix exponential techniques.
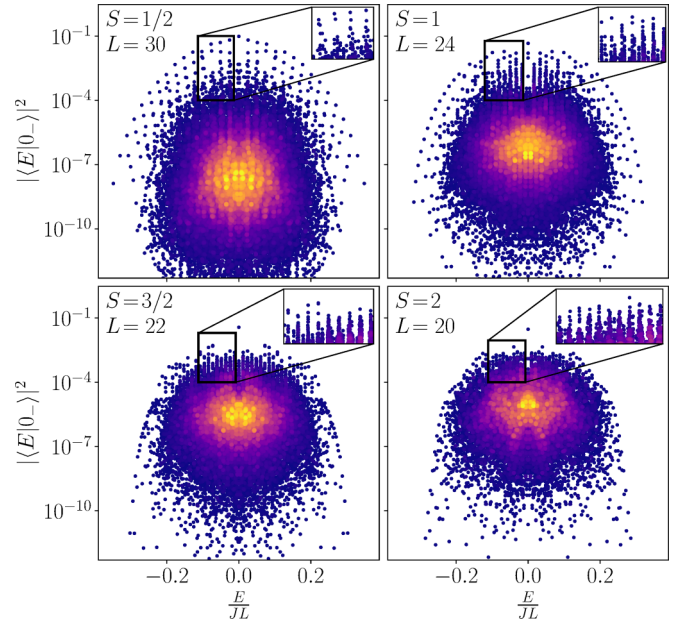

FIG. 1. Quantum many-body scars in the spin-S U(1) QLM: Overlap of the *extreme vacuum* $|0_-\rangle$ with the eigenstates of the quench spin-S U(1) QLM Hamiltonian (1) at $\mu = g = 0$. At all considered values of S, distinctive towers of eigenstates arise that are equally spaced in energy (see insets). These are a hallmark of quantum many-body scars. These results are obtained by exact diagonalization calculations, where L denotes the number of matter sites, and periodic boundary conditions are employed. The color indicates the density of data points, with yellow color representing higher density. In all cases, the Hilbert space has more than 4×10^5 states, with at least 2.5×10^4 states belonging to the relevant symmetry sectors of the extreme vacua.

Resonant scarring. The *physical vacuum* of $\hat{H}$ is its ground state at $\mu \to \infty$ and $g^2 > 0$. In the case of half-integer S, there are two doubly degenerate physical vacua. These can be defined on a two-site two-link unit cell using as quantum numbers the eigenvalues σ_j^z and $s_{j,j+1}^z$ of the matter and electric field operators $\hat{\sigma}_j^z$ and $\hat{s}_{j,j+1}^z$, respectively, explicitly reading as $|\sigma_1^z, s_{1,2}^z, \sigma_2^z, s_{2,3}^z\rangle = |+1, \pm\frac{1}{2}, -1, \pm\frac{1}{2}\rangle$. For integer S, the physical vacuum is nondegenerate, and reads as $|\sigma_1^z, s_{1,2}^z, \sigma_2^z, s_{2,3}^z\rangle = |+1, 0, -1, 0\rangle$. Henceforth, we will denote $|0_+\rangle = |+1, +\frac{1}{2}, -1, +\frac{1}{2}\rangle$ for half-integer S and $|0_+\rangle = |+1, 0, -1, 0\rangle$ for integer S, with the subscript denoting the sign of g^2.

On the other hand, the *extreme vacua* of $\hat{H}$ are high-energy states that can be realized as doubly degenerate ground states of Eq. (1) at $\mu \to \infty$ and $g^2 < 0$: $|\sigma_1^z, s_{1,2}^z, \sigma_2^z, s_{2,3}^z\rangle = |+1, \pm S, -1, \pm S\rangle$. Henceforth, we will denote $|0_-\rangle = |+1, +S, -1, +S\rangle$, with the subscript again indicating the sign of g^2.

We will further consider the charge-proliferated state, which is the ground state of Eq. (1) at $\mu \to -\infty$ and $g^2 > 0$. For half-integer S, it is nondegenerate and reads as $|\text{CP}\rangle = |-1, -\frac{1}{2}, +1, +\frac{1}{2}\rangle$. For integer S, we obtain two doubly degenerate ground states: $|\text{CP}\rangle = |-1, -1, +1, 0\rangle$ and $|-1, 0, +1, +1\rangle$.
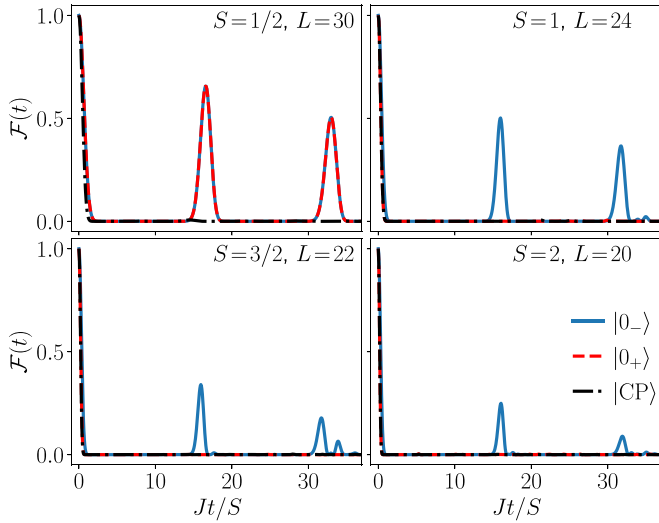
FIG. 2. Dynamics of the fidelity in the wake of a quench by the spin-S U(1) QLM (1) at $\mu = g = 0$ starting in either the extreme vacuum $|0_-\rangle$ (solid blue curve), the physical vacuum $|0_+\rangle$ (dashed red curve), or the charge-proliferated state $|CP\rangle$ (dashed-dotted black curve). The qualitative conclusion is that regardless of the value of S, prominent revivals appear in the fidelity dynamics only when the initial state is the extreme vacuum, whereas for other states the dynamics is thermal. Note that for $S = \frac{1}{2}$, the physical and extreme vacua are identical.
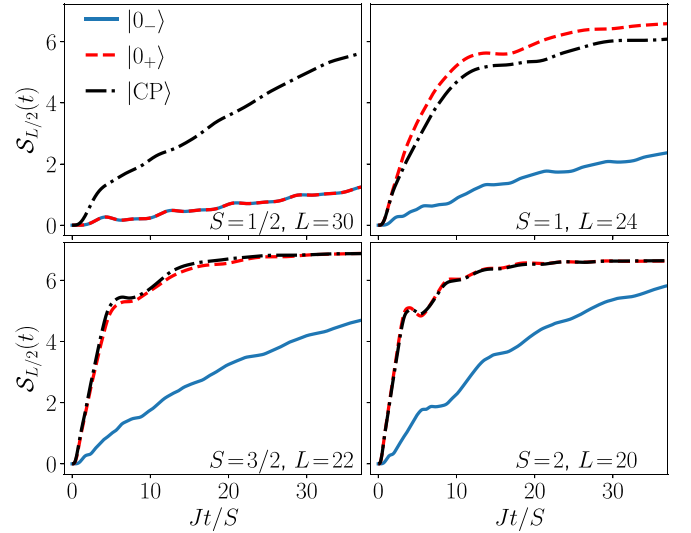

FIG. 3. Dynamics of the mid-chain entanglement entropy for the same quench and initial states considered in Fig. 2. For all considered values of the link spin length S, an anomalously low and slowly growing entanglement entropy arises when the initial state is the extreme vacuum. Preparing the system in the charge-proliferated state or the physical vacuum leads to a fast growth in the entanglement entropy except for the case of $S = \frac{1}{2}$, where the physical and extreme vacua are the same.

With respect to the eigenstates of Hamiltonian (1) at $\mu = g = 0$, we find through ED that only $|0_-\rangle$ exhibits the overlap behavior indicative of scarring for general S (see Fig. 1). Just as in the known case of $S = \frac{1}{2}$, we also see at other values of S signatures of $2SL + 1$ towers equally spaced in energy (see insets), exhibiting large overlap with $|0_-\rangle$, particularly in the middle of the spectrum. The overlap of the top band of states can be further enhanced by considering a truncated version of the QED gauge field [67]. Note how for all values of S that we consider, there is a prominent zero-energy mode with the largest overlap. The presence of these eigenstates is evidence of weak ergodicity breaking in the model. Due to the scaling term $1/\sqrt{S(S + 1)}$, the ground-state energy E_0 is approximately independent of S at $\mu = g^2 = 0$, and we find numerically that $E_0 \approx -0.32L$. As the spectrum is symmetric around zero, we can use this along with the number of towers to get the approximate energy spacing between towers as $\Delta E \approx -2E_0/(2SL) \approx 0.32/S$. We note that the various approximation schemes for scarred eigenstates in the PXP model also show good results for QLMs with larger S [67].

The presence of scarred eigenstates can be detected using the global quench: the system is prepared in some initial state $|\psi(0)\rangle$ and let to evolve under unitary dynamics, $|\psi(t)\rangle = e^{-i\hat{H}t}|\psi(0)\rangle$, generated by the Hamiltonian $\hat{H}$. The state $|\psi(0)\rangle$ is a highly nonequilibrium state, i.e., it is a superposition of a large number of eigenstates of $\hat{H}$, resulting in complex dynamics that we characterize using the fidelity, $\mathcal{F}(t) = |\langle\psi(0)|\psi(t)\rangle|^2$. In the case of $S = \frac{1}{2}$, $|0_+\rangle = |0_-\rangle$, as the last term of Eq. (1) is an inconsequential energy constant since $(\hat{s}_{j,j+1}^z)^2 = \mathbb{1}$. Quenching this vacuum state with $\hat{H}$ at $\mu = 0$ is known to lead to scarring behavior for $S = \frac{1}{2}$ [1,33], and this is exhibited in the revivals of the fidelity, shown in the top left panel of Fig. 2. For comparison, we have included the fidelity dynamics for $|\psi(0)\rangle = |CP\rangle$, which shows no revivals, in agreement with what is established in the literature for this quench when $S = \frac{1}{2}$ [26].

However, once the link spin length is $S > \frac{1}{2}$, we find that the fidelity dynamics exhibits revivals only when the system is initialized in the extreme vacuum $|\psi(0)\rangle = |0_-\rangle$, whereas neither the physical vacuum $|0_+\rangle$ nor the charge-proliferated state $|CP\rangle$ give rise to scarring behavior; see Fig. 2 for $S = 1, \frac{3}{2}, 2$. We have checked that the other vacua $|\sigma_1^z, s_{1,2}^z, \sigma_2^z, s_{2,3}^z\rangle = |+1, \pm M, -1, \pm M\rangle$ with $\frac{1}{2} < M < S$ and higher-energy charge-proliferated states are also not scarred states [67]. From the previous estimate of the energies of scarred towers, we expect the revival period to be $T \approx 6.25\pi S$. However, in practice the energy spacing between towers varies throughout the spectrum. So the relevant energy spacing is the one near $E = 0$, where the scarred states have the higher overlap with $|0_-\rangle$. This provides an estimate of $T \approx 5.13\pi S$, which agrees much more accurately with the numerical data.

We explore the effect of scarring on the dynamics of the mid-chain entanglement entropy $\mathcal{S}_{L/2}(t)$, shown in Fig. 3 for $S = \frac{1}{2}$ to 2. $\mathcal{S}_{L/2}$ is defined as the von Neumann entropy for the reduced density matrix describing one half of the chain. In all cases, starting in the extreme vacuum leads to an anomalously low $\mathcal{S}_{L/2}(t)$ exhibiting significantly slower growth, whereas preparing the system in the charge-proliferated state leads to a rapid increase of the entanglement entropy. Except for the case of $S = \frac{1}{2}$ where the extreme and physical vacua are the same, starting in the physical vacuum leads to qualitatively similar behavior to that of the charge-proliferated state, with a rapid growth in $\mathcal{S}_{L/2}(t)$. These findings are consistent with
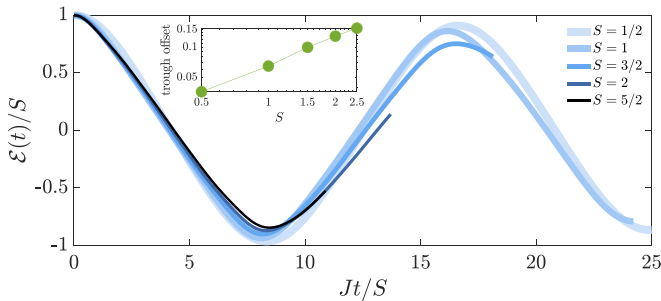
FIG. 4. Dynamics of the electric flux (3) in the TL for a resonant quench ($\mu = g = 0$) starting in the extreme vacuum for different values of S. Inset shows the difference between -1 and the first minimum of the normalized electric flux, plotted as a function of S.

nonthermal scarred dynamics only when the initial state is prepared in the extreme vacuum.

We now investigate the fate of scarring in the thermodynamic limit (TL). Using infinite matrix product states [69], which work directly in the TL, we calculate the dynamics of the electric flux

$$\mathcal{E}(t) = \frac{1}{L} \sum_{j=1}^{L} \langle \psi(t)| \, \hat{s}^{z}_{j,j+1} \, |\psi(t) \rangle, \qquad (3)$$

which is an order parameter associated with the global $\mathbb{Z}_2$ symmetry of the Hamiltonian (1). The corresponding results are shown in Fig. 4. Due to the computational cost of these simulations, where convergence is achieved at a maximal bond dimension of 550 and a time step of $0.0005/J$, we can only reach relatively short times. Nevertheless, scarred revivals in $\mathcal{E}(t)$ are clearly visible in Fig. 4 at all accessible values of S.

To quantify ergodicity breaking, in the inset to Fig. 4 we plot the deviation of the first minimum in $\mathcal{E}(t)$ from -1 as a function of S. For sufficiently large S, we expect the data to saturate to some well-defined value between 0 (perfect scarring) and 1 (full thermalization). While the available values remain far from 1, the deviation clearly grows with S, indicating a weakening of scarring towards the Kogut-Susskind limit $S \to \infty$. At the same time, there is no convergence of the data with respect to S, implying that larger values of S are needed in order to reach a reliable conclusion about the existence of ergodicity breaking in the $S \to \infty$ limit.

As such, we have demonstrated that for a quench at $\mu = g = 0$, the spin-S U(1) QLM (1) exhibits scarring behavior when the system is initially prepared in an *extreme vacuum*. The underlying scarring mechanism is precession of a "large" spin of magnitude SL [70]. The relation between scarring and the Hilbert space constraint can be firmed up by studying the structure of the adjacency graph of the Hamiltonian [67]. These extreme vacua are product states that can be naturally explored in SQM experiments [50,51] even though they are otherwise inaccessible in lattice QED.

Detuned scarring. In a recent study [7], it has been shown theoretically and demonstrated experimentally that there are scarring regimes beyond the resonant one discussed above. This was demonstrated in the spin-$\frac{1}{2}$ U(1) QLM by starting
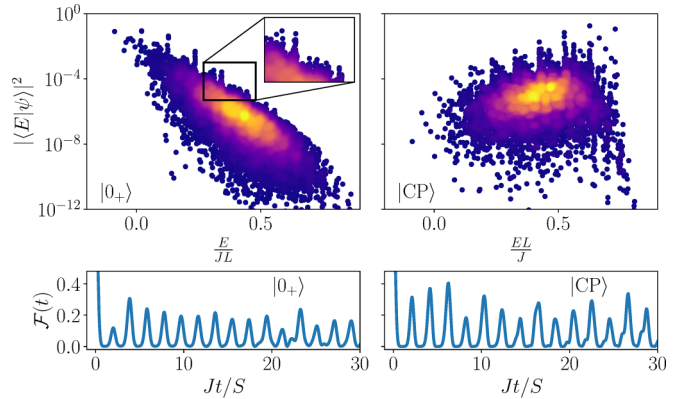

FIG. 5. The spin-S U(1) QLM also exhibits detuned scarring [7], where the physical vacuum $|0_+\rangle$ and the charge-proliferated state $|\mathrm{CP}\rangle$ can lead to scarred dynamics when quenched by Hamiltonian (1) at small nonzero values of μ and g^2. Here, we set $\mu = 0.486J$ and $g^2 = 0.6J$, and the overlap of each of $|0_+\rangle$ and $|\mathrm{CP}\rangle$ with the corresponding eigenstates of Hamiltonian (1) are shown for $L = 20$ and $S = \frac{3}{2}$. Towers of eigenstates equally spaced in energy emerge, indicating the presence of QMBS. We confirm this picture by calculating the dynamics of the fidelity in the wake of this quench. For all accessible evolution times, we find consistent revivals in the fidelity, strongly indicative of scarred dynamics. The color indicates the density of data points, with yellow color representing higher density.

in the charge-proliferated state and performing a quench at finite mass (detuning).

Motivated by the question as to whether QMBS persist in lattice QED for physically relevant initial states, we explore these *detuned* scarring regimes in the spin-$\frac{3}{2}$ U(1) QLM starting in either the physical vacuum $|0_+\rangle$ or the charge-proliferated state $|\mathrm{CP}\rangle$. As shown in Fig. 5, the overlap of these initial states with the eigenstates of the quench Hamiltonian (1) at $\mu = 0.486J$ and $g^2 = 0.6J$ shows distinctive towers equally spaced in energy, similar to the known case of $S = \frac{1}{2}$ [7]. Also displayed in Fig. 5 is the fidelity dynamics for each of $|0_+\rangle$ and $|\mathrm{CP}\rangle$ upon quenching them with this Hamiltonian, where we see persistent revivals up to all considered evolution times. We also arrive at a similar picture for other values of S, and in fact we find a wide range of values of (μ, g^2) over which scarring behavior emerges [67].

Given that $|0_+\rangle$ and $|\mathrm{CP}\rangle$ are both physically relevant in lattice QED in one spatial dimension, and since the latter has been shown to be achieved at relatively small values of S both in [68,71,72] and out of equilibrium [73], our results suggest that QMBS may play a role for understanding dynamics in physically interesting regimes as well.

Summary. In conclusion, we have demonstrated an abundance of QMBS in the paradigmatic spin-S U(1) QLM, a staple of modern SQM experiments on lattice gauge theories. We have shown that the regime of resonant scarring for quenches at zero mass, prevalent in the literature in the case of $S = \frac{1}{2}$, is also present in the case of $S > \frac{1}{2}$ when the system is initially prepared in an *extreme vacuum*, where the local electric field takes on its largest possible eigenvalue. This has been demonstrated by ergodicity-breaking properties of many-body eigenstates, obtained using ED, as well as by showing the existence of quantum revivals in local observables in the TL

using infinite matrix product state method. The extreme vacua associated are not physical as ground states in lattice QED, but they are product states easily implementable in SQM experiments [48,57]. These experiments, in particular, could provide key insight into the persistence of ergodicity breaking upon approaching the limit $S \to \infty$, which our classical simulations cannot reliably access.

We have also presented evidence of detuned scarring in the spin-S U(1) QLM arising from quenches at small nonzero mass and electric-field coupling, when the system is initially prepared in either the physical vacuum, where the local electric field takes on its lowest possible eigenvalue, or the charge-proliferated state. While the scarring phenomenology is similar to the resonant case, the initial states associated with detuned scarring are physically relevant as low-energy states in lattice QED. Given that recent works have shown convergence to the latter limit in and out of equilibrium already at $S \gtrsim \frac{3}{2}$, our results suggest that this detuned scarring regime may already exist in lattice QED.

---

[1] H. Bernien, S. Schwartz, A. Keesling, H. Levine, A. Omran, H. Pichler, S. Choi, A. S. Zibrov, M. Endres, M. Greiner, V. Vuletić, and M. D. Lukin, Probing many-body dynamics on a 51-atom quantum simulator, Nature (London) **551**, 579 (2017).

[2] S. Moudgalya, S. Rachel, B. A. Bernevig, and N. Regnault, Exact excited states of nonintegrable models, Phys. Rev. B **98**, 235155 (2018).

[3] H. Zhao, J. Vovrosh, F. Mintert, and J. Knolle, Quantum Many-Body Scars in Optical Lattices, Phys. Rev. Lett. **124**, 160604 (2020).

[4] H. Zhao, A. Smith, F. Mintert, and J. Knolle, Orthogonal Quantum Many-Body Scars, Phys. Rev. Lett. **127**, 150601 (2021).

[5] D. Bluvstein, A. Omran, H. Levine, A. Keesling, G. Semeghini, S. Ebadi, T. T. Wang, A. A. Michailidis, N. Maskara, W. W. Ho, S. Choi, M. Serbyn, M. Greiner, V. Vuletić, and M. D. Lukin, Controlling quantum many-body dynamics in driven Rydberg atom arrays, Science **371**, 1355 (2021).

[6] P. N. Jepsen, Y. K.-E. Lee, H. Lin, I. Dimitrova, Y. Margalit, W. W. Ho, and W. Ketterle, Long-lived phantom helix states in Heisenberg quantum magnets, Nat. Phys. **18**, 899 (2022).

[7] G.-X. Su, H. Sun, A. Hudomal, J.-Y. Desaules, Z.-Y. Zhou, B. Yang, J. C. Halimeh, Z.-S. Yuan, Z. Papić, and J.-W. Pan, Observation of many-body scarring in a Bose-Hubbard quantum simulator, Phys. Rev. Res. **5**, 023010 (2023).

[8] P. Zhang, H. Dong, Y. Gao, L. Zhao, J. Hao, J.-Y. Desaules, Q. Guo, J. Chen, J. Deng, B. Liu, W. Ren, Y. Yao, X. Zhang, S. Xu, K. Wang, F. Jin, X. Zhu, B. Zhang, H. Li, C. Song *et al.*, Many-body Hilbert space scarring on a superconducting processor, Nat. Phys. **19**, 120 (2022).

[9] S. Moudgalya, N. Regnault, and B. A. Bernevig, Entanglement of exact excited states of Affleck-Kennedy-Lieb-Tasaki models: Exact results, many-body scars, and violation of the strong eigenstate thermalization hypothesis, Phys. Rev. B **98**, 235156 (2018).

[10] C.-J. Lin and O. I. Motrunich, Exact Quantum Many-Body Scar States in the Rydberg-Blockaded Atom Chain, Phys. Rev. Lett. **122**, 173401 (2019).

[11] C. J. Turner, A. A. Michailidis, D. A. Abanin, M. Serbyn, and Z. Papić, Weak ergodicity breaking from quantum many-body scars, Nat. Phys. **14**, 745 (2018).

[12] M. Schecter and T. Iadecola, Weak Ergodicity Breaking and Quantum many-body Scars in Spin-1 XY Magnets, Phys. Rev. Lett. **123**, 147201 (2019).

[13] W. W. Ho, S. Choi, H. Pichler, and M. D. Lukin, Periodic Orbits, Entanglement, and Quantum Many-Body Scars in Constrained Models: Matrix Product State Approach, Phys. Rev. Lett. **122**, 040603 (2019).

[14] C. J. Turner, A. A. Michailidis, D. A. Abanin, M. Serbyn, and Z. Papić, Quantum scarred eigenstates in a Rydberg atom chain: Entanglement, breakdown of thermalization, and stability to perturbations, Phys. Rev. B **98**, 155134 (2018).

[15] M. Srednicki, Chaos and quantum thermalization, Phys. Rev. E **50**, 888 (1994).

[16] J. M. Deutsch, Quantum statistical mechanics in a closed system, Phys. Rev. A **43**, 2046 (1991).

[17] M. Rigol, V. Dunjko, and M. Olshanii, Thermalization and its mechanism for generic isolated quantum systems, Nature (London) **452**, 854 (2008).

[18] J. Eisert, M. Friesdorf, and C. Gogolin, Quantum many-body systems out of equilibrium, Nat. Phys. **11**, 124 (2015).

[19] L. D'Alessio, Y. Kafri, A. Polkovnikov, and M. Rigol, From quantum chaos and eigenstate thermalization to statistical mechanics and thermodynamics, Adv. Phys. **65**, 239 (2016).

[20] J. M. Deutsch, Eigenstate thermalization hypothesis, Rep. Prog. Phys. **81**, 082001 (2018).

[21] D. K. Mark, C.-J. Lin, and O. I. Motrunich, Unified structure for exact towers of scar states in the Affleck-Kennedy-Lieb-Tasaki and other models, Phys. Rev. B **101**, 195131 (2020).

[22] S. Moudgalya, N. Regnault, and B. A. Bernevig, η-pairing in Hubbard models: From spectrum generating algebras to quantum many-body scars, Phys. Rev. B **102**, 085140 (2020).

[23] N. O'Dea, F. Burnell, A. Chandran, and V. Khemani, From tunnels to towers: Quantum scars from Lie algebras and q-deformed Lie algebras, Phys. Rev. Res. **2**, 043305 (2020).

[24] K. Pakrouski, P. N. Pallegar, F. K. Popov, and I. R. Klebanov, Many-Body Scars as a Group Invariant Sector of Hilbert Space, Phys. Rev. Lett. **125**, 230602 (2020).

[25] N. Shiraishi and T. Mori, Systematic Construction of Counterexamples to the Eigenstate Thermalization Hypothesis, Phys. Rev. Lett. **119**, 030601 (2017).

[26] M. Serbyn, D. A. Abanin, and Z. Papić, Quantum many-body scars and weak breaking of ergodicity, Nat. Phys. **17**, 675 (2021).

[27] S. Moudgalya, B. A. Bernevig, and N. Regnault, Quantum many-body scars and Hilbert space fragmentation: A review of exact results, Rep. Prog. Phys. **85**, 086501 (2022).

[28] A. Omran, H. Levine, A. Keesling, G. Semeghini, T. T. Wang, S. Ebadi, H. Bernien, A. S. Zibrov, H. Pichler, S. Choi, J. Cui, M. Rossignolo, P. Rembold, S. Montangero, T. Calarco, M. Endres, M. Greiner, V. Vuletić, and M. D. Lukin, Generation and manipulation of Schrödinger cat states in Rydberg atom arrays, Science **365**, 570 (2019).

[29] S. Dooley, Robust quantum sensing in strongly interacting systems with many-body scars, PRX Quantum **2**, 020330 (2021).

[30] J.-Y. Desaules, F. Pietracaprina, Z. Papić, J. Goold, and S. Pappalardi, Extensive Multipartite Entanglement from su(2) Quantum Many-Body Scars, Phys. Rev. Lett. **129**, 020601 (2022).

[31] S. Dooley, S. Pappalardi, and J. Goold, Entanglement enhanced metrology with quantum many-body scars, Phys. Rev. B **107**, 035123 (2023).

[32] M. Brenes, M. Dalmonte, M. Heyl, and A. Scardicchio, Many-Body Localization Dynamics from Gauge Invariance, Phys. Rev. Lett. **120**, 030601 (2018).

[33] F. M. Surace, P. P. Mazza, G. Giudici, A. Lerose, A. Gambassi, and M. Dalmonte, Lattice Gauge Theories and String Dynamics in Rydberg Atom Quantum Simulators, Phys. Rev. X **10**, 021041 (2020).

[34] D. Banerjee and A. Sen, Quantum Scars from Zero Modes in an Abelian Lattice Gauge Theory on Ladders, Phys. Rev. Lett. **126**, 220601 (2021).

[35] A. S. Aramthottil, U. Bhattacharya, D. González-Cuadra, M. Lewenstein, L. Barbiero, and J. Zakrzewski, Scar states in deconfined $\mathbb{Z}_2$ lattice gauge theories, Phys. Rev. B **106**, L041101 (2022).

[36] S. Biswas, D. Banerjee, and A. Sen, Scars from protected zero modes and beyond in U(1) quantum link and quantum dimer models, SciPost Phys. **12**, 148 (2022).

[37] S. Weinberg, *The Quantum Theory of Fields*, Vol. 2: Modern Applications (Cambridge University Press, Cambridge, 1995).

[38] C. Gattringer and C. Lang, *Quantum Chromodynamics on the Lattice: An Introductory Presentation*, Lecture Notes in Physics (Springer, Berlin, 2009).

[39] A. Zee, *Quantum Field Theory in a Nutshell* (Princeton University Press, Princeton, NJ, 2003).

[40] R. P. Feynman and P. Cziffra, *Quantum Electrodynamics*, A Lecture Note and Reprint Series (Basic Books, New York, 1962).

[41] E. A. Martinez, C. A. Muschik, P. Schindler, D. Nigg, A. Erhard, M. Heyl, P. Hauke, M. Dalmonte, T. Monz, P. Zoller, and R. Blatt, Real-time dynamics of lattice gauge theories with a few-qubit quantum computer, Nature (London) **534**, 516 (2016).

[42] C. Muschik, M. Heyl, E. Martinez, T. Monz, P. Schindler, B. Vogell, M. Dalmonte, P. Hauke, R. Blatt, and P. Zoller, U(1) Wilson lattice gauge theories in digital quantum simulators, New J. Phys. **19**, 103020 (2017).

[43] N. Klco, E. F. Dumitrescu, A. J. McCaskey, T. D. Morris, R. C. Pooser, M. Sanz, E. Solano, P. Lougovski, and M. J. Savage, Quantum-classical computation of Schwinger model dynamics using quantum computers, Phys. Rev. A **98**, 032331 (2018).

[44] A. Keesling, A. Omran, H. Levine, H. Bernien, H. Pichler, S. Choi, R. Samajdar, S. Schwartz, P. Silvi, S. Sachdev, P. Zoller, M. Endres, M. Greiner, V. Vuletić, and M. D. Lukin, Quantum Kibble–Zurek mechanism and critical dynamics on a programmable Rydberg simulator, Nature (London) **568**, 207 (2019).

[45] C. Kokail, C. Maier, R. van Bijnen, T. Brydges, M. K. Joshi, P. Jurcevic, C. A. Muschik, P. Silvi, R. Blatt, C. F. Roos, and P. Zoller, Self-verifying variational quantum simulation of lattice models, Nature (London) **569**, 355 (2019).

[46] F. Görg, K. Sandholzer, J. Minguzzi, R. Desbuquois, M. Messer, and T. Esslinger, Realization of density-dependent Peierls phases to engineer quantized gauge fields coupled to ultracold matter, Nat. Phys. **15**, 1161 (2019).

[47] C. Schweizer, F. Grusdt, M. Berngruber, L. Barbiero, E. Demler, N. Goldman, I. Bloch, and M. Aidelsburger, Floquet approach to $\mathbb{Z}2$ lattice gauge theories with ultracold atoms in optical lattices, Nat. Phys. **15**, 1168 (2019).

[48] A. Mil, T. V. Zache, A. Hegde, A. Xia, R. P. Bhatt, M. K. Oberthaler, P. Hauke, J. Berges, and F. Jendrzejewski, A scalable realization of local U(1) gauge invariance in cold atomic mixtures, Science **367**, 1128 (2020).

[49] N. Klco, M. J. Savage, and J. R. Stryker, SU(2) non-Abelian gauge field theory in one dimension on digital quantum computers, Phys. Rev. D **101**, 074512 (2020).

[50] B. Yang, H. Sun, R. Ott, H.-Y. Wang, T. V. Zache, J. C. Halimeh, Z.-S. Yuan, P. Hauke, and J.-W. Pan, Observation of gauge invariance in a 71-site Bose–Hubbard quantum simulator, Nature (London) **587**, 392 (2020).

[51] Z.-Y. Zhou, G.-X. Su, J. C. Halimeh, R. Ott, H. Sun, P. Hauke, B. Yang, Z.-S. Yuan, J. Berges, and J.-W. Pan, Thermalization dynamics of a gauge theory on a quantum simulator, Science **377**, 311 (2022).

[52] I. Bloch, J. Dalibard, and W. Zwerger, Many-body physics with ultracold gases, Rev. Mod. Phys. **80**, 885 (2008).

[53] W. S. Bakr, J. I. Gillen, A. Peng, S. Fölling, and M. Greiner, A quantum gas microscope for detecting single atoms in a Hubbard-regime optical lattice, Nature (London) **462**, 74 (2009).

[54] U.-J. Wiese, Ultracold quantum gases and lattice systems: Quantum simulation of lattice gauge theories, Ann. Phys. (Berlin) **525**, 777 (2013).

[55] M. C. Bañuls, R. Blatt, J. Catani, A. Celi, J. I. Cirac, M. Dalmonte, L. Fallani, K. Jansen, M. Lewenstein, S.

Montangero, C. A. Muschik, B. Reznik, E. Rico, L. Tagliacozzo, K. Van Acoleyen, F. Verstraete, U.-J. Wiese, M. Wingate, J. Zakrzewski, and P. Zoller, Simulating lattice gauge theories within quantum technologies, Eur. Phys. J. D **74**, 165 (2020).

[56] Y. Alexeev, D. Bacon, K. R. Brown, R. Calderbank, L. D. Carr, F. T. Chong, B. DeMarco, D. Englund, E. Farhi, B. Fefferman, A. V. Gorshkov, A. Houck, J. Kim, S. Kimmel, M. Lange, S. Lloyd, M. D. Lukin, D. Maslov, P. Maunz, C. Monroe *et al.*, Quantum computer systems for scientific discovery, PRX Quantum **2**, 017001 (2021).

[57] M. Aidelsburger, L. Barbiero, A. Bermudez, T. Chanda, A. Dauphin, D. González-Cuadra, P. R. Grzybowski, S. Hands, F. Jendrzejewski, J. Jünemann, G. Juzeliūnas, V. Kasper, A. Piga, S.-J. Ran, M. Rizzi, G. Sierra, L. Tagliacozzo, E. Tirrito, T. V. Zache, J. Zakrzewski *et al.*, Cold atoms meet lattice gauge theory, Philos. Trans. R. Soc. A **380**, 20210064 (2022).

[58] E. Zohar, Quantum simulation of lattice gauge theories in more than one space dimension: Requirements, challenges and methods, Philos. Trans. R. Soc. A **380**, 20210069 (2022).

[59] N. Klco, A. Roggero, and M. J. Savage, Standard model physics and the digital quantum revolution: Thoughts about the interface, Rep. Prog. Phys. **85**, 064301 (2022).

[60] L. Homeier, C. Schweizer, M. Aidelsburger, A. Fedorov, and F. Grusdt, $\mathbb{Z}_2$ lattice gauge theories and Kitaev's toric code: A scheme for analog quantum simulation, Phys. Rev. B **104**, 085138 (2021).

[61] S Chandrasekharan and U.-J Wiese, Quantum link models: A discrete approach to gauge theories, Nucl. Phys. B **492**, 455 (1997).

[62] J. Schwinger, Gauge invariance and mass. II, Phys. Rev. **128**, 2425 (1962).

[63] S. Coleman, R. Jackiw, and L. Susskind, Charge shielding and quark confinement in the massive Schwinger model, Ann. Phys. **93**, 267 (1975).

[64] D. Banerjee, M. Dalmonte, M. Müller, E. Rico, P. Stebler, U.-J. Wiese, and P. Zoller, Atomic Quantum Simulation of Dynamical Gauge Fields Coupled to Fermionic Matter: From String Breaking to Evolution after a Quench, Phys. Rev. Lett. **109**, 175302 (2012).

[65] V. Kasper, F. Hebenstreit, F. Jendrzejewski, M. K. Oberthaler, and J. Berges, Implementing quantum electrodynamics with ultracold atomic systems, New J. Phys. **19**, 023030 (2017).

[66] B. Mukherjee, Z. Cai, and W. V. Liu, Constraint-induced breaking and restoration of ergodicity in spin-1 PXP models, Phys. Rev. Res. **3**, 033201 (2021).

[67] J.-Y. Desaules, A. Hudomal, D. Banerjee, A. Sen, Z. Papić, and J. C. Halimeh, Prominent quantum many-body scars in a truncated Schwinger model, Phys. Rev. B **107**, 205112 (2023).

[68] T. V. Zache, M. V. Damme, J. C. Halimeh, P. Hauke, and D. Banerjee, Toward the continuum limit of a (1+1)D quantum link Schwinger model, Phys. Rev. D **106**, L091502 (2022).

[69] U. Schollwöck, The density-matrix renormalization group in the age of matrix product states, Ann. Phys. **326**, 96 (2011).

[70] S. Choi, C. J. Turner, H. Pichler, W. W. Ho, A. A. Michailidis, Z. Papić, M. Serbyn, M. D. Lukin, and D. A. Abanin, Emergent SU(2) Dynamics and Perfect Quantum Many-Body Scars, Phys. Rev. Lett. **122**, 220603 (2019).

[71] B. Buyens, S. Montangero, J. Haegeman, F. Verstraete, and K. Van Acoleyen, Finite-representation approximation of lattice gauge theories at the continuum limit with tensor networks, Phys. Rev. D **95**, 094509 (2017).

[72] M. C. Bañuls and K. Cichy, Review on novel methods for lattice gauge theories, Rep. Prog. Phys. **83**, 024401 (2020).

[73] J. C. Halimeh, M. V. Damme, T. V. Zache, D. Banerjee, and P. Hauke, Achieving the quantum field theory limit in far-from-equilibrium quantum link models, Quantum **6**, 878 (2021).